PCCP

RSC Publishing

PAPER

View Article Online
View Journal | View Issue

Cite this: *Phys. Chem. Chem. Phys.*, 2013, **15**, 11257

Iron cation catalyzed reduction of N_2O by CO: gas-phase temperature dependent kinetics

Joshua J. Melko,[a] Shaun G. Ard,[a] Joseph A. Fournier,[b] Jun Li,[c] Nicholas S. Shuman,[a] Hua Guo,[c] Jürgen Troe[de] and Albert A. Viggiano*[a]

Received 23rd January 2013,
Accepted 2nd May 2013

DOI: 10.1039/c3cp50335f

www.rsc.org/pccp

The ion–molecule reactions $Fe^+ + N_2O \rightarrow FeO^+ + N_2$ and $FeO^+ + CO \rightarrow Fe^+ + CO_2$, which catalyze the reaction $CO + N_2O \rightarrow CO_2 + N_2$, have been studied over the temperature range 120–700 K using a variable temperature selected ion flow tube apparatus. Values of the rate constants for the former two reactions were experimentally derived as k_2 (10^{-11} cm^3 s^{-1}) = 2.0(±0.3) $(T/300)^{-1.5(\pm0.2)}$ + 6.3(±0.9) exp(−515(±77)/T) and k_3 (10^{-10} cm^3 s^{-1}) = 3.1(±0.1) $(T/300)^{-0.9(\pm0.1)}$. Characterizing the energy parameters of the reactions by density functional theory at the B3LYP/TZVP level, the rate constants are modeled, accounting for the intermediate formation of complexes. The reactions are characterized by nonstatistical intrinsic dynamics and rotation-dependent competition between forward and backward fluxes. For $Fe^+ + N_2O$, sextet–quartet switching of the potential energy surfaces is quantified. The rate constant for the clustering reaction $FeO^+ + N_2O + He \rightarrow FeO(N_2O)^+ + He$ was also measured, being k_4 (10^{-27} cm^6 s^{-1}) = 1.1(±0.1) $(T/300)^{-2.5(\pm0.1)}$ in the low pressure limit, and analyzed in terms of unimolecular rate theory.

Introduction

Transition metal compounds are the backbone of many catalysts due to their ability to bind and activate reactant species *via* a change in the oxidation state of the metal center. In gas-phase ion catalysis, the active transition metal species can be studied in an isolated manner, providing a molecular level understanding of the catalytic active sites and reaction mechanisms that take place in the solution or solid state.[1–6] An important example of gas-phase transition metal catalysis was reported by Kappes and Staley in 1981.[7] Their experiments employed ion-cyclotron resonance spectrometry to investigate the Fe^+ catalyzed reduction of nitrous oxide by carbon monoxide. While the overall reaction, depicted below as reaction (1), is highly exothermic (ΔH^0 = −365.5 kJ mol^{-1}),[8] it is not spontaneous at room temperature. However, Kappes and Staley were able to conduct experiments on reactions (2) and (3) shown below, which together represent the overall iron cation catalyzed process depicted in reaction (1).

$$CO + N_2O \rightarrow CO_2 + N_2 \quad \Delta_r H^0 = -365.5 \pm 0.1 \text{ kJ mol}^{-1} \qquad (1)$$

$$Fe^+ + N_2O \rightarrow FeO^+ + N_2 \quad \Delta_r H^0 = -172.2 \pm 1.9 \text{ kJ mol}^{-1} \qquad (2)$$

$$FeO^+ + CO \rightarrow Fe^+ + CO_2 \quad \Delta_r H^0 = -192.6 \pm 1.9 \text{ kJ mol}^{-1} \qquad (3)$$

Kappes and Staley measured the rate constants for reactions (2) and (3) at room temperature, finding 7×10^{-11} cm^3 s^{-1} and 9×10^{-10} cm^3 s^{-1}, respectively.[7] In 1995, Bohme *et al.* conducted selected ion flow tube experiments on reactions (2) and (3), and obtained rate coefficients of 3.1(±0.1) × 10^{-11} cm^3 s^{-1} and 2.05(±0.2) × 10^{-10} cm^3 s^{-1}, respectively.[9] These values have since been remeasured by Bohme *et al.* to be 3.7(±1.1) × 10^{-11} cm^3 s^{-1} and 1.8(±0.7) × 10^{-10} cm^3 s^{-1}, respectively.[10,11] Importantly, the studies also revealed that the FeO^+ ion can cluster with N_2O, depicted in reaction (4), representing a possible poisoning of the overall cycle. However, it was shown that $FeO(N_2O)_n^+$, at least for n = 1–3, readily oxidizes CO to CO_2 as shown in reaction (5), indicating that the cycle is not poisoned by reaction (4).

$$FeO^+ + nN_2O + He \rightarrow FeO(N_2O)_n^+ + He \qquad (4)$$

$$FeO(N_2O)_n^+ + CO \rightarrow Fe^+ + CO_2 + n(N_2O) \qquad (5)$$

Additional experiments on reaction (2) have been performed by Armentrout *et al.*, who have measured the reaction cross

[a] *Air Force Research Laboratory, Space Vehicles Directorate, Kirtland AFB, NM 87117-5776, USA. E-mail: Albert.Viggiano@kirtland.af.mil*
[b] *Sterling Chemistry Laboratory, Yale University, P.O. Box 208107, New Haven, CT 06520, USA*
[c] *Department of Chemistry and Chemical Biology, University of New Mexico, Albuquerque, NM 87131, USA*
[d] *Institut für Physikalische Chemie, Universität Göttingen, Tammannstrasse 6, D-37077 Göttingen, Germany*
[e] *Max-Planck-Institut für Biophysikalische Chemie, D-37077 Göttingen, Germany*

section as a function of ion translational energy.[12] They found that the reaction of Fe^+ with N_2O proceeds with little or no activation energy, but with a cross section of only about 10% of the Langevin collisional cross section.[13] Attempts to explain the low efficiency without an activation energy were made in 1996 by Plane and Rollason, who performed temperature dependent rate constant measurements for reaction (2) using time-resolved laser induced fluorescence.[14] They observed a room temperature rate constant that agreed with that of Bohme *et al.*, but also discovered a positive temperature dependence over a temperature range of 294–773 K. Plane and Rollason reported an activation energy for reaction (2) of 6.2(±1.3) kJ mol^{-1}, in contrast to the results of Armentrout *et al.*, and proposed that the reaction involves vibrationally excited modes of N_2O. A significant portion (11%) of the bending mode of N_2O is excited at room temperature,[14] and thus a mechanism involving vibrationally excited N_2O would explain both the positive temperature dependence[14] and the reaction cross section measurement by Armentrout *et al.*[12]

In the current work, we investigate reactions (2)–(4) over a broad temperature range, from approximately 120 K to 700 K. We confirm the previous room temperature results for reactions (2) and (3), obtaining rate constants of $3.2(\pm0.5) \times 10^{-11}$ cm^3 s^{-1} and $3.1(\pm0.5) \times 10^{-10}$ cm^3 s^{-1}, which correspond to 3.7% and 41% of the respective collision rates. Further, we confirm the room temperature rate constant of reaction (4) for $n = 1$, yielding an effective second-order rate constant of $1.4(\pm0.2) \times 10^{-11}$ cm^3 s^{-1} (at $[He] = 1.3 \times 10^{16}$ cm^{-3}). We present new temperature dependent data for the rate constants of reactions (2)–(4), providing the first measurements for reactions (3) and (4) over any extended temperature range. We also provide a theoretical analysis of the rate constants for reactions (2)–(4) that rationalizes the experimental data. Although a number of questions remain open, the comparison of experiments and modeling provides valuable insight into the intrinsic reaction dynamics of the processes. Interestingly, for reaction (2) our temperature dependent rate constants disagree with the existing measurements of Plane and Rollason. While we provide previously unavailable data below room temperature that shows a negative temperature dependence from 120 K to 300 K, our measurements above room temperature are flat, and do not show the positive dependence observed by Plane and Rollason. We conclude that our data are explained by a reaction path that in part is characterized by a mixing of sextet and quartet potentials through spin–orbit coupling. In this way, the positive activation barrier in the sextet potential can be circumvented by a pathway that does not have a positive activation barrier, a mechanism that has been proposed for many other reactions of Fe^+ and FeO^+.[15–19]

Experimental methods

All measurements were performed on the variable temperature selected ion flow tube instrument located at the Air Force Research Laboratory, which has been described in detail elsewhere.[20] Briefly, Fe^+ ions are created within an electron impact source (at electron energies that varied from 30–250 eV) in the presence of a 10% mixture of $Fe(CO)_5$ in He, with N_2O additionally supplied in the source for the formation of FeO^+. Ions are extracted and injected into a quadrupole mass filter where the desired ion, either Fe^+ or FeO^+, is mass selected. The ions are then focused before introduction into a laminar flow tube *via* a Venturi inlet, where they are quickly thermalized and carried downstream by a He buffer gas. The flow tube is maintained at 0.4 Torr throughout all experiments, except for those involving verification of third order behavior near the low pressure limit (see below). After about 10^4 ion-helium collisions, the neutral reagent (N_2O or CO) is added 59 cm upstream from the end of the flow tube, resulting in reaction times on the order of 4 ms, dependent on both helium buffer flow, which is varied from 10–13 std. L min^{-1}, and temperature. All gas flows are controlled using mass flow controllers.

After traveling the length of the flow tube, the core of the flow is sampled through a truncated nosecone with a 2 mm aperture. The remainder of the flow is pumped away using a roots pump through a throttled gate valve that acts to maintain a constant pressure within the flow tube. After the nosecone, the primary ions and product ions are guided by a lens stack to a quadrupole mass filter for analysis, and are subsequently detected using an electron multiplier. By monitoring the decay of the primary ion as a function of the neutral reagent flow, kinetic data are obtained. Temperature dependencies (from approximately 120 K to 700 K) of rate constants are also measured. The temperatures are attained by either resistively heating the flow tube (300–700 K), pulsed liquid nitrogen (120–220 K), or recirculating methanol chillers (220–300 K).

Since electronic state specific reactivity has been observed in a large number of reactions, including a variety of reactions involving Fe^+,[21–27] we comment on the likelihood of excited state Fe^+ in our system. In a separate study, we have indeed observed that some electronically excited Fe^+ enters the flow tube,[28] which could affect our rate constant measurements for reaction (2) in the current study. For an electron energy of about 50 eV (typical of some of the experiments presented here), it has been shown that one may expect about 40% of the ground electronic state, ^6D, with the remaining contributions primarily from the excited ^4F and ^4D states.[29–31] Additionally, it has been shown that the ^4D state may not be efficiently quenched by helium under experimental conditions similar to ours.[22,29] With the $Fe^+ + N_2O$ rate being slow, we should observe curvature in the decay plots if two states are present and reacted differently. Further, since our electron temperature varied over a large range for the results presented here, we may even observe varying degrees of curvature in the decay plots corresponding to various populations of unquenched excited states. Fig. 1 shows an example of our raw data at two different temperatures. No such curvature was observed for these temperatures, or any temperature we investigated, indicating that the excited states were quenched, or the unquenched states react similarly to the ground state. In any case, our rate constant measurements should represent the ground electronic state, ^6D, and the question is irrelevant to branching since there is only one product.

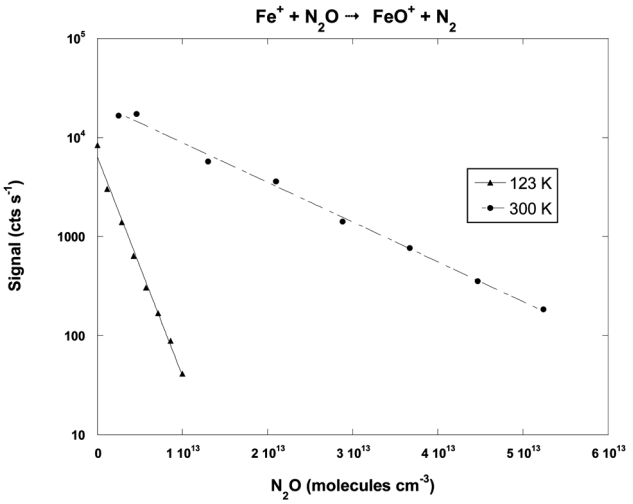

Fig. 1 Parent ion decay plots for reaction (2) at 123 K and 300 K.

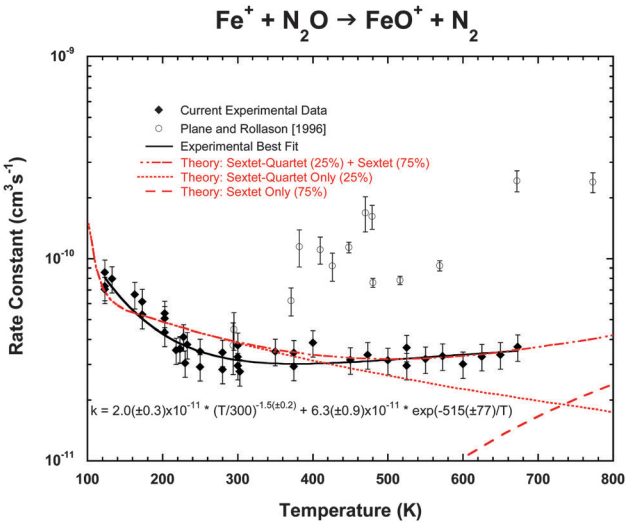

Fig. 2 Rate constant as a function of temperature for reaction (2). Diamonds denote data from the current study (with error bars at ±15%) and open circles denote data from the literature.[14] The best fit line through our experimental data is depicted as a solid black line (from 123–673 K), and the equation for this line is given at the bottom of the figure. The red lines (from 100 to 800 K) show the results of preliminary modeling: the dotted red line denotes the contribution from the sextet–quartet reaction channel, the dashed red line denotes the contribution from the sextet only reaction channel, and the dash-dotted red line is the sum of both the sextet–quartet and sextet only pathways, see the text.

A comment on spin–orbit states within a given electronic state also bears mentioning. Weisshaar *et al.* have shown spin–orbit state effects on Fe^+ reactivity.[32,33] However, we are unable to separate the different reactivities of spin–orbit states (if indeed they are different for reaction (2)) within the ^6D level. While it is conceivable that in our experiment the spin–orbit states may quench to the ground state, $^6D_{9/2}$, it seems more likely that the states interconvert with the many helium collisions, giving us a thermal distribution of the spin–orbit states within a given level. If the spin–orbit states reacted very differently and were not interconverting, we should see curvature in our decay plots as the distribution of states changes, which we do not. We conclude that we likely have a thermal distribution of spin–orbit states, though we cannot rule out that we have only the $^6D_{9/2}$ ground state.

Experimental results and discussion

The rate constants measured for reactions (2) and (3) at room temperature under pseudo-first order conditions (*i.e.* $[N_2O]$ or $[CO] \gg [Fe^+]$ or $[FeO^+]$) are in excellent agreement with those previously published.[7,9–11,14] At room temperature, reaction (2) proceeds with a rate constant of $3.2(\pm0.5) \times 10^{-11}$ cm^3 s^{-1}, which is 3.7% of its collision rate (see Table 1) given by the Su–Chesnavich equation.[34] The temperature dependence of this rate constant (Fig. 2) is remarkably flat between 230–670 K, while rising sharply below 230 K. This type of behavior appears unusual, possibly unique, over such a broad temperature range for reactions with an efficiency this low. An empirical best-fit line through our data is shown that consists of two terms. The first is a straightforward power dependence that is common to ion-molecule reactions of this type, and accounts for the negative temperature dependence from 120 K to 250 K. The second part of the fit is in Arrhenius form. Together, the fit can reproduce the sharp T dependence that flattens out at higher temperature where the Arrhenius behavior counters the negative temperature dependence. We later explore the theoretical basis of this behavior.

Also plotted in Fig. 2 are the previous results of Plane and Rollason from 1996. The disagreement is striking between our measured flat dependence and their positive temperature dependence from room temperature to 700 K. It is important to note that the experiments by Plane and Rollason probe a specific spin–orbit level of the ground electronic state, namely the $^6D_{9/2}$ state, with time-resolved laser induced fluorescence. As discussed above, we believe our experiments sample the Maxwell–Boltzmann distribution of spin–orbit levels within the ^6D state at the flow tube temperature. It is conceivable that the different levels that are sampled could lead to the difference in observed temperature dependence (and spin–orbit specific reactivity has been shown for Fe^+ in the literature[32,33]). If we assume that the $^6D_{9/2}$ reacts and all other states are unreactive, we can estimate the maximum rate constant for that state.

Table 1 Rate constant, collision rate constant, and reaction efficiency at 300 K for reactions (2) and (3). Error in our rate constant measurement is estimated at ±15%. The most recent literature values[10] are shown in brackets

Reaction	k (300 K) cm^3 s^{-1}	k_{coll} (300 K) cm^3 s^{-1}	Reaction efficiency k/k_{coll} (300 K)
$Fe^+ + N_2O \rightarrow FeO^+ + N_2$	$3.2(\pm0.5) \times 10^{-11}$ [$3.7(\pm1.1) \times 10^{-11}$]	8.6×10^{-10}	0.037
$FeO^+ + CO \rightarrow Fe^+ + CO_2$	$3.1(\pm0.5) \times 10^{-10}$ [$1.8(\pm0.7) \times 10^{-10}$]	7.6×10^{-10}	0.41

Even with the increase, our values above room temperature are still about a factor of two below the results of Plane and Rollason, and the shape of the temperature dependence is much less sharp. Thus, we conclude the difference is not due to the difference in spin–orbit states sampled. We speculate that the positive temperature dependence observed by Plane and Rollason was due to the unavoidable competing reactions present in their experiments, which were performed without a mass spectrometer. Their explanation of the positive temperature dependence is contingent upon excitation of the bending vibrational mode in N_2O, which is 11.1% populated at 295 K.[14] This could explain the roughly 10% efficiency that Armentrout *et al.* observed, if the ground state does not react and the vibrationally excited N_2O reacts with no barrier. Based on work by Jalink *et al.*,[35] Plane and Rollason propose a pathway in which the vibrational excitation allows for a non-adiabatic transition from the sextet surface onto a quartet surface that is exothermic by 83 kJ mol^{-1}. Fig. 3 illustrates the energetics of the reaction pathway as calculated in the present work (for more details, see below), where the sextet and quartet surfaces represent spin–orbit averages of the ^{6}D and ^{4}F states, respectively. This pathway, which qualitatively agrees with those present in the literature,[10,11,36] shows the sextet–quartet transition and need not involve reactions of vibrationally excited N_2O, as we discuss below in a modeling of the reaction rate.

Our temperature dependent rate constants for reaction (3) are shown in Fig. 4. We point out that the FeO^+ used in this reaction was produced in the source, not from the prior reaction, and should be quenched to the ground state. Our experience over many years shows that only diatomics with excited energies much higher than that present here are unquenched. The room temperature rate constant we find for reaction (3) of $3.1(\pm0.5) \times 10^{-10}$ is only slightly higher than previous results.[8–10,37] In Table 1 we also provide the collision rate and the room temperature reaction efficiency (defined as the ratio of the rate constant to the ion-molecule collision rate). The overall temperature dependence goes roughly as T^{-1}, as is typical for ion-molecule reactions that proceed at less than the collision rate.

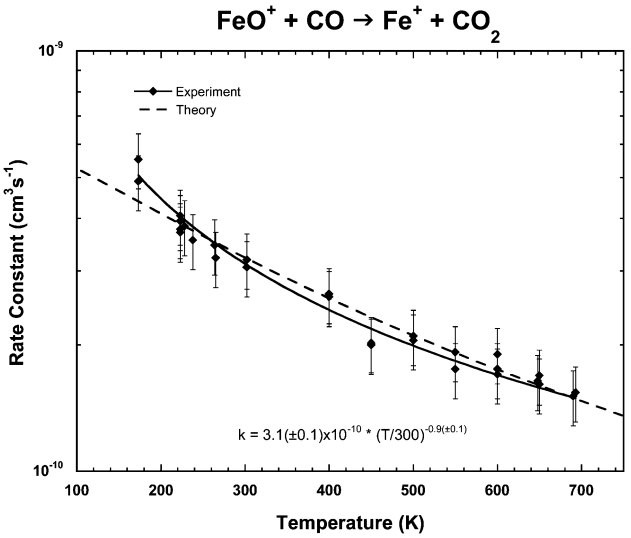

Fig. 4 Rate constant as a function of temperature for reaction (3). Diamonds denote data from the current study (with error bars at ±15%). The best fit line through our experimental data is depicted as a solid line (from 173–693 K), and the equation for this line is given at the bottom of the figure. The dashed line (from 100 to 750 K) gives our preliminary modeling results, see the text.

To further understand this temperature dependence, we have again calculated the energy profile along the reaction pathway, as shown in Fig. 5. We note that only the sextet reaction pathway is shown, since the quartet state $^4FeO^+$ is 61 kJ mol^{-1} higher in energy than the $^6FeO^+$ ground state and sextet stationary points are significantly lower in energy than the quartet ones (*e.g.* ^{6}INT 1 is 68.5 kJ mol^{-1} below ^{4}INT 1, ^{6}INT 2 is 92.9 kJ mol^{-1} below ^{4}INT 2). In agreement with others,[10,22,36,38] we show that the iron atom in FeO^+ approaches the carbon side of CO to form a linear intermediate. The reaction then proceeds through a transition state that is just slightly exothermic, where the oxygen atom in FeO^+ is rotated into position, and subsequently forms a second linear intermediate from which CO_2 leaves. We note that others[36] have indicated a direct pathway from reactants to the second intermediate, where the oxygen side of FeO^+ approaches the carbon atom of CO. We were unable to locate this channel. If this second channel were the main pathway, one might expect the reaction to proceed at near the collision rate with little

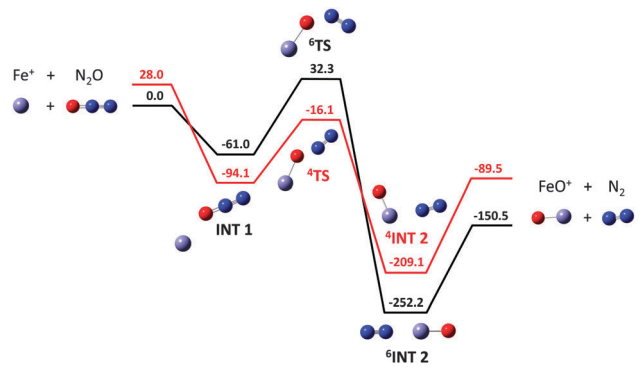

Fig. 3 Reaction pathway for reaction (2) computed using DFT with the B3LYP functional and the TZVP basis set. The surface corresponding to the sextet state is in black, while the surface corresponding to the quartet state is in red. Surfaces represent averages of the spin–orbit states. Energies listed are in kJ mol^{-1} relative to the sextet surface reactants.

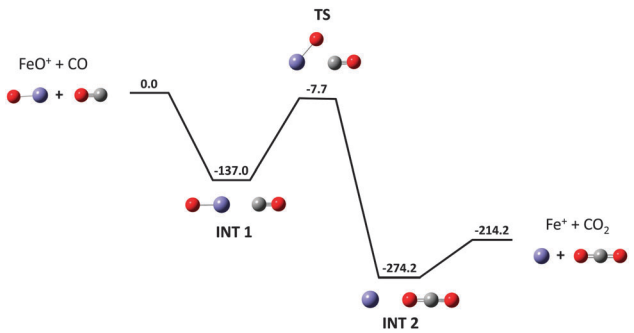

Fig. 5 Spin–orbit averaged sextet reaction pathway for reaction (3) computed using DFT with the B3LYP functional and the TZVP basis set. Energies listed are in kJ mol^{-1} relative to the reactants.

temperature dependence. We believe that both pathways may occur, but our measured rate and temperature dependence are more consistent with at least some of the reactions proceeding through an intrinsic barrier on the way to products. Additional discussion is provided in the modeling section below.

Our results for reactions (2) and (3) show that the iron cation catalyzed reduction of N_2O by CO is most facile at lower temperature, where both reactions have a higher rate constant and therefore larger reaction efficiency, in particular reaction (2). Fig. 6 shows a plot of the coupled reaction efficiencies (*i.e.* the product of the reaction efficiencies for reactions (2) and (3), as defined in the literature[10]) as a function of temperature. Note that the overall efficiency roughly doubles when the temperature is dropped from 300 K to 200 K. This contradicts previous findings[14] suggesting that the rate of reaction (2) increases with temperature, which would result in an increased reaction efficiency at elevated temperatures.

Important for any catalytic cycle is the threat of poisoning the active material with unwanted side-reactions or products. Previously, Bohme *et al.* have noted that the FeO^+ ion can associate with an additional N_2O molecule to form clusters, as shown in reaction (4).[9] While this could potentially prevent CO oxidation, which restores the cycle-starting Fe^+ ion, Bohme *et al.* have shown that at room temperature the adducts (at least for $n \leq 3$) oxidize CO to CO_2 with close to the same rate coefficient as FeO^+.[9] Thus, the cycle is not poisoned upon formation of the $FeO(N_2O)_n^+$ species, and upon oxidizing CO, the clusters liberate nN_2O molecules and reform Fe^+, as shown in reaction (5). We have begun to explore the temperature dependence of this process and show in Fig. 7 and Table 2 our results for the third-order rate constants of reaction (4), for $n = 1$ formation. We represent our data as third order rate constants; deviations from the low pressure third order limit of reaction (4) are estimated to be less than 10 percent for the applied pressure of 0.4 Torr. We confirm the room temperature rate constant obtained by Bohme *et al.*;[9] additionally, we find that the rate constant for the reaction scales with temperature as $T^{-2.5}$. This temperature dependence of reaction (4) (for $n = 1$) can be rationalized by standard unimolecular rate theory, as shown below. We hope to explore reaction (4) also for the higher order adducts (*i.e.* $n = 2$ and 3), as well as reaction (5), but note that at the present time creating the higher order adducts in the source results in too low an ion signal. Together, these temperature dependencies would provide a more detailed understanding of the competing processes shown in reactions (2)–(5), which should lead to a better estimation of the temperature required for optimum efficiency of iron cation catalyzed N_2O reduction by CO.

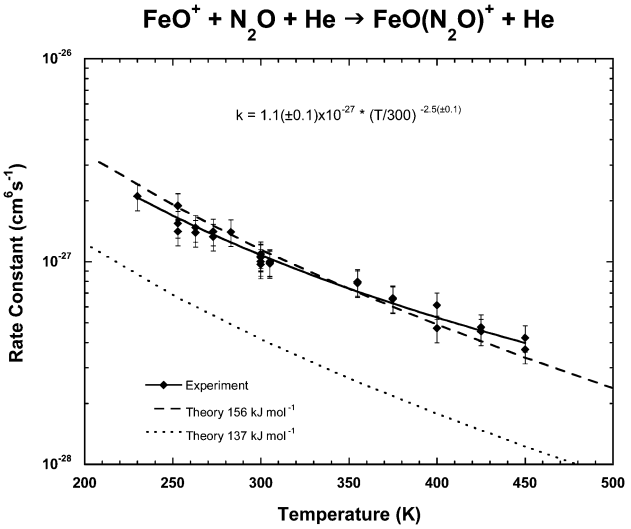

Fig. 7 Third order rate constant (at [He] $\approx 1.3 \times 10^{16}$ cm^{-3}) as a function of temperature for reaction (4). Diamonds denote data from the current study (with error bars at ±15%). The best fit line through our experimental data is depicted as a solid line (from 230–450 K), and the equation for this line is given at the top of the figure. The dashed lines are theoretical results from unimolecular rate theory (the upper curve assumes an adduct bond energy of about 156 kJ mol^{-1}, while the lower curve assumes an adduct bond energy of 137 kJ mol^{-1}, see the text).

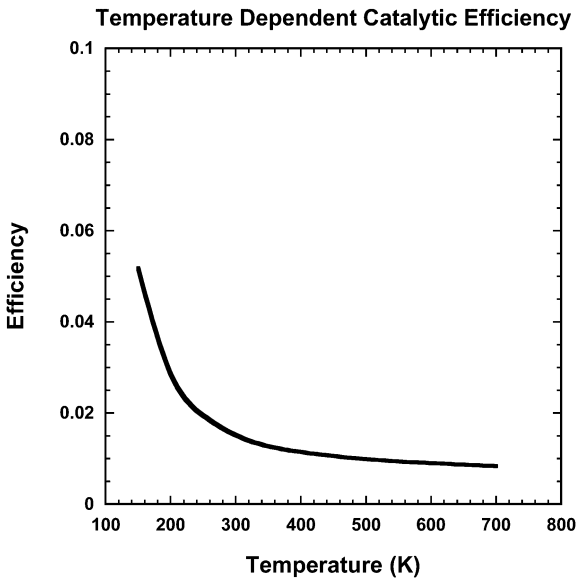

Fig. 6 Temperature dependent catalytic efficiency for the iron cation catalyzed reduction of N_2O by CO. Catalytic efficiency is defined here as the product of the individual reaction efficiencies for reactions (2) and (3).

Modeling of the rates of reactions (2) and (3)

In order to characterize the dynamics of reactions (2) and (3) and to model their rates, we have performed density functional theory (DFT) calculations at the B3LYP/TZVP level.[39,40] To test the suitability of the DFT theory, we have calculated the spin–orbit averaged splitting between the ground sextet and excited quartet states of Fe^+ using the CASSCF,[41] CASPT2,[42] and UCCSD(T) methods.[43] The B3LYP/TZVP methodology was chosen because it gives a value of 28.0 kJ mol^{-1} for the splitting, which is close to the UCCSD(T) value of 35.1 kJ mol^{-1} and the experimental value of 23.8 kJ mol^{-1}.[44,45] We are aware that this DFT approach can only be qualitative and for more quantitative results multireference calculations would be required. However, the DFT approach often provides a useful general picture of the

Table 2 Second-order rate constant (k_{bi}), helium number density, and third-order rate constant (k_{ter}) at 300 K for reaction (4) (n = 1). Error in our rate constant measurement is estimated at ±15%. The most recent literature value[9] is shown in brackets

Reaction	k_{bi} (300 K) cm^3 s^{-1}	[He] cm^{-3}	k_{ter} (300 K) cm^6 s^{-1}
$FeO^+ + N_2O$ +He → $FeO(N_2O)^+$ + He	$1.4(\pm0.2) \times 10^{-11}$ [$1.2(\pm0.1) \times 10^{-11}$]	1.3×10^{16}	$1.1(\pm0.2) \times 10^{-27}$

intrinsic reaction mechanism. Nevertheless, the calculated energies only provide a first orientation and they are adapted in the modeling as empirical fit parameters.

Keeping in mind the limitations of the DFT approach, the stationary points along the reaction paths on both the quartet and sextet states have been identified and their harmonic frequencies calculated. Results are qualitatively similar to previous calculations in the literature;[10,11,36,38] for the most part there are only small quantitative differences in barrier heights. The transition states were confirmed to have a single imaginary frequency, and intrinsic reaction coordinate (IRC) calculations were performed to confirm their correlation to the reactants and products. The geometries, energies, and frequencies obtained are listed in Tables 3–6, with comparisons to available experimental data. All calculations were performed using the Gaussian 09 package.[46]

Fig. 3 shows the results for reaction (2). We show two potentials to be accounted for, a sextet potential starting from the electronic ground state $Fe^+(^6D)$ levels and a quartet potential starting from excited state $Fe^+(^4F)$. We emphasize that these reflect averages of the spin–orbit states, in actuality there are manifolds of the two potentials, that are mixed to varying extents along the pathway. Here, we adopt a simplified picture where we use the spin–orbit averaged energies of the various stationary points along the sextet and quartet potentials that allows for a treatment of the temperature dependent kinetics. Due to spin–orbit coupling, reaction (2), starting on the sextet potential, either remains on that potential or switches to the quartet potential. With fine structure splittings for $Fe^+(^6D)$ on the order of several hundred cm^{-1},[44,45,47] which are related to spin–orbit couplings treated by Landau–Zener theory, one expects a substantial probability for transition from the sextet to the quartet potential when $Fe^+(^6D)$ approaches N_2O. As we are not in the position to quantify this transition probability, we leave it as an empirical fit parameter for branching between sextet and quartet pathways. We note that spin-forbidden dissociation reactions like those of N_2O and CS_2,[47,48] with fine-structure splittings for $O(^3P)$ and $S(^3P)$ of similar magnitude to $Fe^+(^6D)$, also proceed with substantial transition probabilities for spin-switching (thermally averaged values between 0.01 for N_2O and 0.1 for CS_2). Nevertheless, spin–orbit coupling in general will vary along the reaction coordinate (see *e.g.* the reaction between FeO^+ and CH_4)[15] such that conclusions about the branching on the basis of spin–orbit coupling of the separated reactants may be inconclusive. According to the preceding discussion, we expect partial sextet–quartet spin-switching

Table 4 Calculated harmonic frequencies (in cm^{-1}) of the stationary points for the reaction $Fe^+ + N_2O \rightarrow FeO^+ + N_2$ at the sextet and quartet electronic states. Experimental values from the literature are also shown

		Frequency					
Species		1	2	3	4	5	6
Sextet state							
Reactants	Expt.[58]	589[a]	1285	2224			
	This work	587[a]	1327	2350			
INT 1	This work	84	205	534	550	1237	2383
TS	This work	−858	55	94	368	482	2140
INT 2	This work	93[a]	238[a]	270	812	2465	
Products	Expt.[59]		2358.57				
	This work	831	2461				
Quartet state							
INT 1	This work	84	269	530	547	1269	2403
TS	This work	−556	142	278	457	663	1992
INT 2	This work	117	243	265	333	911	2455
Products	This work	966	2461				

[a] Doubly degenerate.

Table 3 Optimized geometries (all lengths r in angstroms, angles θ and φ in degrees) and rotational constants (B_1, B_2, B_3 in cm^{-1}) of the stationary points for the reaction $Fe^+ + N_2O \rightarrow FeO^+ + N_2$ at the sextet and quartet electronic states. Experimental values from the literature are also shown

Species		$r_{NN'}$	$r_{N'O}$	r_{OFe}	$\theta_{NN'O}$	$\theta_{N'OFe}$	$\varphi_{NN'OFe}$	B_1	B_2	B_3
Sextet state										
Reactants	Expt.[58]	1.128	1.184		180.0			0.419		
	This work	1.123	1.185		180.0			0.423		
INT 1	This work	1.111	1.212	2.220	178.7	144.8	180.0	3.094	0.058	0.057
TS	This work	1.113	1.489	1.834	143.1	134.9	0.0	1.063	0.077	0.072
INT 2	This work	1.092	3.765	1.648	180.0	0.0		1.546		
Products	Expt.[59]	1.098						—		
								1.998		
	This work	1.093		1.641				0.503		
								2.017		
Quartet state										
INT 1	This work	1.111	1.210	2.034	177.8	144.2	180.0	3.318	0.065	0.064
TS	This work	1.127	1.447	1.822	140.2	84.4	180.0	0.786	0.110	0.097
INT 2	This work	1.093	2.819	1.570	143.2	43.5	180.0	0.632	0.110	0.094
FeO^+	This work			1.560				0.557		

Table 5 Optimized geometries (all lengths r in angstroms, angles θ and φ in degrees) and rotational constants (B_1, B_2, B_3 in cm^{-1}) of the stationary points for the reaction $FeO^+ + CO \rightarrow Fe^+ + CO_2$ at the sextet electronic state. Experimental values from the literature are also shown

Species		r_{OFe}	r_{CO}	$r_{CO'}$	θ_{FeOC}	$\theta_{OCO'}$	$\varphi_{FeOCO'}$	B_1	B_2	B_3
Reactants	Expt.[58]			1.128				—		
								1.931		
	This work	1.641		1.127				0.503		
								1.937		
INT 1	This work	1.656	3.798	1.114	0.0	180.0		0.070		
TS	This work	1.769	1.748	1.132	78.2	124.8	180.0	0.693	0.104	0.090
INT 2	This work	2.237	1.179	1.142	180.0	180.0		0.051		
Products	Expt.[58,59]		1.160	1.160		180.0		0.390		
	This work		1.161	1.161		180.0		0.391		

Table 6 Calculated harmonic frequencies (in cm^{-1}) of the stationary points for the reaction $FeO^+ + CO \rightarrow Fe^+ + CO_2$ at the sextet electronic state. Experimental values from the literature are also shown

		Frequency					
Species		1	2	3	4	5	6
Reactants	Expt.[58]		2169.81				
	This work	831	2219				
INT 1	This work	100[a]	276	288[a]	787	2329	
TS	This work	−570	161	211	356	716	2127
INT 2	This work	46	175	649	655	137	2448
		63					
Products	Expt.[59]	667[a]	1333	2349			
	This work	675[a]	1377	2420			

[a] Doubly degenerate.

for reaction (2) (with an efficiency to be derived from the experiments) while part of the reaction proceeds on the sextet potential without spin-switching. The reaction begins *via* the intermediate formation of an $(Fe\text{-}ONN)^+$ complex (INT 1, with both states having similar structures), which proceeds over an $(FeONN)^{+\neq}$ transition state (^{6}TS or ^{4}TS) to a second $(OFe\text{-}NN)^+$ complex (^{6}INT 2 or ^{4}INT 2), finally leading to $FeO^+ + N_2$. According to Fig. 3, there may or may not be a switch from the initial sextet potential to the quartet potential on the way to INT 1. This has consequences for the relevant barrier of the reaction which is either at a positive or negative energy relative to the reactants. The problem of spin-switching does not arise for reaction (3) where the reaction proceeds on a single sextet potential, see Fig. 5 and accompanying discussion.

With the intermediate formation of the complexes INT 1, reactions (2) and (3) belong to the class of complex-forming bimolecular reactions[49] which cannot be treated by ordinary transition state theory. In order to model these reactions it is crucial to consider both the energy (E)- and the angular momentum (J)-dependencies of cross sections and specific rate constants. In this case there may be "rotational channel switching".[49–51] By this term we mean the rotation-dependent competition between forward and backward fluxes over intrinsic TS barriers. Because of the much smaller effective rotational constant of the system at the loose entrance to the complex INT 1 (denoted by subscript a) compared to the rigid exit from the complex at TS (denoted by subscript b) even a "potential reef" (or "submerged barrier") of TS may become a barrier with an energy higher than the entrance barrier as J is increased. In other words, at low J the centrifugal barriers at the entrance ($E_{0a}(J)$) may be higher than the barriers at the exit ($E_{0b}(J)$), while the opposite is true for larger J. There is a second rotational effect. The potential minimum of INT 1 will increase in energy with increasing J and finally cease to exist; the reaction then will switch from complex-forming to direct character.

We consider a bimolecular reaction $B + C \Leftrightarrow A^* \rightarrow$ products with the possibility of competition between forward flux $A^* \rightarrow$ products and backward flux $A^* \rightarrow B + C$ of the excited complex A^*. The rate constant for product formation is then given by[49,52,53]

$$k = \frac{k_B T}{h}\left(\frac{h^2}{2\pi\mu k_B T}\right)^{3/2} \frac{Q_{el}(A)Q^*}{Q_{el}(B)Q_{el}(C)Q_{vibrot}(B)Q_{vibrot}(C)} \quad (6)$$

with

$$Q^* = \sum_i g_i \exp(-E_{0a_i}/k_B T)\, Y_i \quad (7)$$

where Q_{el} and Q_{vibrot} are the electronic and rovibrational partition functions, Q^* is the total pseudopartition function of the activated complex, μ is the reduced mass, i denotes all quantum states (with degeneracy g_i) of the colliding pair $B + C$, E_{0a_i} are the corresponding threshold energies at the entrance for complex formation and the yields Y_i are the ratios of forward/(backward + forward) fluxes leading to products.

For a capture-controlled process, the Y_i would be equal to unity. If, in addition, the E_{0a_i} would be determined by a long-range ion-dipole potential, one would have

$$E_{0a_i}(l) = [l(l+1)\hbar^2/2\mu - q\mu_D]^2/2\alpha q^2 + E_{vibrot,i}(B) + E_{vibrot,i}(C) \quad (8)$$

(the term in brackets being zero for $l(l+1) \leq 2\mu\mu_D q/\hbar^2$; l denotes the orbital angular momentum quantum number, q the ion charge, α the polarizability, and μ_D the dipole moment of the neutral). Evaluating Q^* from eqn (7) then leads to

$$Q^* = Q_{vibrot}(B)Q_{vibrot}(C)\sum_{J=0}^{\infty}(2l+1)\exp[-E_{0a}(l)/k_B T] \quad (9)$$

with $E_{0a}(l)$ given by the first term on the right hand side of eqn (8). This finally gives[52,53] the locked dipole-rate constant

$$k = k_L + 2\pi q\mu_D(2/\pi\mu kT)^{1/2} \quad (10)$$

with the Langevin rate constant

$$k_L = 2\pi q(\alpha/\mu)^{1/2} \quad (11)$$

Accounting for the anisotropy of the ion-permanent dipole potential using the statistical adiabatic channel model[53] or using classical trajectory calculations[34,53] modifies the $E_{0a}(l)$ and introduces a dipole-locking factor into the second term on the right hand side of eqn (10) well approximated by the Su–Chesnavich equation.[34,53]

The determination of the reaction yield factor Y_i in eqn (7) requires insight into the intrinsic reaction dynamics of the intermediate complex INT 1. If INT 1 is internally coupled sufficiently strongly, and if the potential well of INT 1 is sufficiently deep, statistical theory may apply.[49] With specific rate constants $k_a(E,J) = W_a(E,J)/h\rho(E,J)$ and $k_b(E,J) = W_b(E,J)/h\rho(E,J)$ for backward (a) and forward (b) dissociations of INT 1, the Y_i then would be characterized by

$$Y(E,J) = W_b(E,J)/[W_a(E,J) + W_b(E,J)] \quad (12)$$

where $W(E,J)$ are the numbers of open channels as a function of total energy, E, and angular momentum, J, of INT 1. For the rigid exit activated complex TS, $W_b(E,J)$ would be calculated by Rice–Ramsperger–Kassel–Marcus (RRKM) theory[54] including overall rotation, using the TS parameters given in Tables 3–6. For a loose entrance such as in an ion-induced dipole system, $W_a(E,J)$ would be derived from phase space theory (PST) such as elaborated elsewhere.[55] In this case, $W_a(E,J)$ increases much more strongly with increasing energy than $W_b(E,J)$ such that $Y(E,J)$ would be a decreasing function of the energy E. For the present system, we found that statistical theory with full mixing of the vibrations of the reactants with rotations and orbital motion leads to a much too strong back flux and highly underestimates the rate constants. Even by lowering the TS barrier to the energy minimum of INT 1, the rigid activated complex character of TS would be responsible for a much too large backward flux from rotating INT to the reactants. Therefore, we abandoned the statistical approach using eqn (12) and proceeded to a nonstatistical approach such as described in the following.

A full calculation of the yield function $Y(E,J)$ beyond statistical theory would require the knowledge of the complete potential energy surface. On this surface, zero-point energy-corrected trajectory calculations would have to be made, which is far beyond the scope of the present work, in particular as the DFT calculations are only of semiquantitative character (see above). Instead we attempted a simplified modeling with the following properties of the $Y(E,J)$. We assumed that the vibrational quantum states of the reactants are conserved during the passage from the entrance a to the exit b, and do not participate in energy randomization. We assumed that large ranges of l are important such that $J \approx l$. We use $E_{0a}(J)$ from eqn (8) and employ

$$E_{0b}(J) \approx E_{0b}(J = 0) + B^{\neq}J(J + 1) \quad (13)$$

with the effective rotational constant $B^{\neq} = (B_2 + B_3)/2$ for TS from Tables 3 and 5, and $E_{0b}(J = 0)$ from Fig. 3 and 5. If $E_{0a}(J) < E_{0b}(J)$, we put $Y(E,J) \approx 0$, as this range would practically correspond to a direct, single transition state, process with a much more rigid activated complex and much smaller contribution to the rate constant than relevant for the range of J-values with $E_{0a}(J) > E_{0b}(J)$. If $E_{0a}(J) > E_{0b}(J)$, we put $Y(E,J) = 0$ as long as $E < E_{0a}(J)$, because then the complex INT 1 cannot be entered; if $E > E_{0a}(J)$, the complex can be entered and $Y(E,J)$ is governed by the competition between forward and backward fluxes. In this case we represent $Y(E,J)$ by a function which decreases with increasing energy like in statistical theory, in which the back flux with increasing energy wins over the forward flux. We tentatively assume

$$Y(E,J) \approx \exp(-E/\gamma) \quad (14)$$

with an empirical fit parameter γ proportional to $E_{0a}(J) - E_{0b}(J)$, which is represented by $\gamma \approx \gamma_0[E_{0a}(J) - E_{0b}(J)]$. We emphasize that eqn (14) at this stage is empirical and should be verified by classical trajectory calculations on an appropriate potential energy surface. We then calculate Q^* from eqn (7) both with the modeled $Y(E,J)$ and with $Y(E,J) = 1$, and we identify the ratio $Q^*/Q^*(Y = 1)$ with the ratio k/k^{S-Ch}, where k^{S-Ch} denotes the Su–Chesnavich ion-dipole capture rate constant.[34,53] We replace the summation over i in Q^* by a summation over J and an integration over E with the density of orbital and rotational states, $\rho(E,J)$, as given by PST.[55] For the linear + linear reactant system $FeO^+ + CO$, at large J, *e.g.*, one has $\rho(E,J) = E/B_{FeO^+}B_{CO}$, while for the atom + linear reactant system $Fe^+ + N_2O$ one has $\rho(E,J) = 1/B_{N_2O}$.

By fitting the parameter γ_0 and reducing the DFT value of the TS energy slightly, we could reasonably well represent the experimental results for the $FeO^+ + CO$ reaction. As usual for complex-forming bimolecular reactions,[49] the negative temperature coefficient of the rate constant is attributed to the fact that the TS energy increases with increasing J much stronger than the centrifugal energy barrier for formation of INT 1, such that the back dissociation of INT 1 gains importance with increasing temperature. Fig. 4 demonstrates the comparison of experiment and modeling. Although the modeling is still preliminary in the sense that we have not undertaken trajectory calculations, the results look encouraging. Compared to the Langevin capture constant $k_L = 7.3 \times 10^{-10}$ cm^3 s^{-1}, the reduction of the rate constant is due to the described rotational channel switching. Optimum results of our fitting were obtained with $\gamma_0 \approx 1$ and using a TS energy of -14 kJ mol^{-1}. (Increasing γ_0 by a factor of 2 would have increased k_3 (100 K) by a factor of 1.1 while k_3 (700 K) would have increased by a factor of 3.3; on the other hand, for $\gamma_0 = 1$, putting the TS energy at -7.7 kJ mol^{-1}, k_3 (100 K) would change by a factor of 0.7 while k_3 (700 K) would change by a factor of 0.3.)

Analyzing reaction (2) requires additional considerations on the two-channel character of the reaction, the spin-switching sextet–quartet channel with the rate constant $k_{2,SQ}$ and the spin-conserving sextet channel with $k_{2,SS}$. For simplicity, we assume that the thermally averaged sextet–quartet transition probability f_{SQ} is only weakly temperature dependent (similar to the analysis[47,48] of the spin-forbidden dissociation of N_2O and

CS_2 in terms of Landau–Zener theory). f_{SQ} is then treated as a temperature independent fit parameter and k_2 expressed as

$$k_2 = f_{SQ}k_{2,SQ} + (1 - f_{SQ})k_{2,SS} \quad (15)$$

$k_{2,SQ}$ is modeled using eqn (6)–(14), similar to the analysis of k_3. Since $k_{2,SS}$ increases from only 0.02 $k_{2,SQ}$ at 400 K to 0.47 $k_{2,SQ}$ at 800 K, the parameters γ_0 and f_{SQ} can be fitted independent of $k_{2,SS}$ from the low temperature value of k_2 at $T < 400$ K. We obtain $\gamma_0 \approx 1$ as for reaction (3) and $f_{SQ} \approx 0.25$. Because of the high sextet energy barrier at TS, there is no rotational channel switching for the sextet channel. In this case, we put $Y(E,J) \approx 1$ for all $E > E_{0b}(J)$ and we change the DFT value of the sextet TS energy to a value of 25.8 kJ mol^{-1}. (In this case, for temperature below 400 K, k_2 is directly proportional to f_{SQ}; increasing γ_0 by a factor of 2, here increases $k_{2,SQ}$ (100 K) by a factor of 1.05, while $k_{2,SQ}$ (400 K) increases by a factor of 1.3 and $k_{2,SQ}$ (700 K) by a factor of 3.5. With the chosen value of γ_0, the experimental temperature dependence of k_2 for temperatures below 400 K is reasonably well reproduced, see Fig. 2; a contribution from the sextet channel becomes visible only at higher temperatures. Retaining the sextet TS energy at the DFT value of 32.3 kJ mol^{-1} would reduce $k_{2,SS}$ at 700 K by a factor of 25 and thus eliminate the upturn of k_2 at higher temperatures, see Fig. 2.) The modeled value of k_2 is compared with the experiments in Fig. 2, also shown are the contributions from the two mechanisms (*i.e.* 25% sextet–quartet and 75% sextet only). In spite of the preliminary character of the modeling, the results appear to be insightful, since the back flux parameter $\gamma_0 \approx 1$ is of similar value for reactions (2) and (3) and the fitted sextet–quartet transition probability $f_{SQ} \approx 0.25$ appears to be of reasonable order of magnitude. The small absolute value of k_2 now is attributed to the partly spin-forbidden character of the sextet–quartet channel and the large positive activation energy of the sextet channel. The steep negative temperature coefficient at low T arises from rotational channel switching during complex formation. The flat temperature dependence of k_2 at $T > 300$ K is due to the compensation of the decrease of k_{SQ} by the increase of k_{SS} with increasing temperature.

Modeling of the rate of reaction (4)

We finally provide a modeling of the rate constant k_4 (for $n = 1$) in its low-pressure, third-order, limit. We follow the formalism of standard unimolecular rate theory,[54] employing the estimated molecular parameters of the adduct $FeO(N_2O)^+$ from DFT calculations (see Table 7). Within the uncertainties of the input parameters given, both the absolute values and temperature dependence of k_4 can be reproduced. Fig. 7 compares the modeling results to experimental data. Neglecting weak collision effects, our first attempt at modeling led to $k_{4,0}$ (*i.e.*, the limiting low pressure rate constant for reaction (4)) that reproduces the shape of the temperature dependence but produced a 300 K value that is a factor of 2.7 lower than the experimental result. An increase in the adduct bond strength from the DFT value of 137 to 156 kJ mol^{-1} would account for the discrepancy, a value well within the estimated error. However, uncertainties in the molecular parameters used in the calculations could also be responsible for the difference. Given the uncertainties, the results illustrated in Fig. 7 appear satisfactory. At low temperature, the rate constants approach about 5% of the Langevin rate constant, k_L, for capture of N_2O by FeO^+ ($k_L = 7.81 \times 10^{-10}$ cm^3 s^{-1}). Thus, one should inspect for the falloff behavior[54] in reaction (4). At 300 K, the "center of the falloff curve" $[He]_c$ (where the reaction changes from a third-order to a second-order process) should be located near $[He]_c \approx 8 \times 10^{17}$ cm^{-3}. Deviations from the third order ($k_4/k_{4,0} < 0.9$), therefore, are estimated[54] to occur at $[He]/[He]_c > 10^{-2}$, *i.e.* at $[He] > 10^{16}$ cm^{-3}, corresponding to about 0.3 Torr, *i.e.* barely visible in the present data. $[He]_c$ increases with increasing temperature. The estimates of $k_{4,0}$ (for $n > 1$) and the shapes of falloff curves given elsewhere[56] should allow one to predict deviations from the second and the third order of k_4 for the sequence of clustering reactions shown in reaction (4) (see the example[57] of hydration reactions of NO^+).

Table 7 Estimated anharmonicity factor F_{anh}, dissociation energy D (in kJ mol^{-1} at 0 K), rotational constant B_1 (in cm^{-1}), and harmonic frequencies (in cm^{-1}) for $FeO^+(N_2O)$ from DFT calculations

			Frequency						
F_{anh}	D	B_1	1	2	3	4	5	6	7
1.66	136.8	0.040	77[a]	158[a]	272	615[a]	828	1452	2434

[a] Doubly degenerate.

Conclusions

We have studied the temperature dependence of the rate constants for the reactions $Fe^+ + N_2O$ and $FeO^+ + CO$, which represent the two half-reactions in the iron cation catalyzed reduction of N_2O by CO. Additionally, we have studied the temperature dependence of the side reaction, $FeO^+ + N_2O$. We confirm the room temperature rate constants observed in the literature, while most of the temperature dependent data represent the first measurements of their kind (the exception being $Fe^+ + N_2O$ above room temperature). Our present results show that the overall efficiency for the iron cation catalyzed reduction of N_2O by CO decreases quite sharply with temperature, which is largely governed by the temperature dependence of the $Fe^+ + N_2O$ reaction.

The derived values for the rate constant of $Fe^+ + N_2O$, k_2, are rationalized in terms of complex formation in two reaction channels, one switching from a sextet to a quartet potential and one staying on a sextet potential. The fitted sextet–quartet transition probability of about 1/4 is of the order of magnitude expected for "spin-forbidden" reactions of this type.[47,48] The two-channel character of the reaction results in an unusual temperature dependence of k_2. At low temperature the spin-switching sextet–quartet channel dominates, because it does not involve positive energy barriers on the way from reactants to products. The rate of this channel has a negative temperature coefficient, as is typical for complex-forming bimolecular reactions with "submerged energy barriers" that show "rotational channel switching", *i.e.* back flux from the intermediate

complex to the primary reactants,[49] which gains importance with increasing temperature. In our work, the extent of back flux was found to be much less pronounced than given by statistical unimolecular rate theory[49] such that a parameterized nonstatistical description had to be formulated; a more detailed analysis awaits further work. At high temperatures the additional sextet channel starts to contribute. This channel has a relatively high activation barrier with positive energy. The sum of the contributions from the two channels can be made responsible for the unusual temperature dependence with a marked negative temperature coefficient at low temperatures ($T \leq 200$ K) and a broad flat plateau at medium temperatures (200–500 K). The modeling predicts the transition to a positive temperature coefficient at higher temperatures. Slight indications of this transition may have been seen experimentally (at $T \geq 500$ K). The marked positive temperature coefficient of k_2 for $T \geq 300$ K suggested in other experiments[14] could not be confirmed in the present work.

The reaction of $FeO^+ + CO$ showed the typical behaviour of a complex-forming bimolecular reaction[49] with a submerged energy barrier on the way from the complex to the products, *i.e.* rotational channel switching and back-flux to the reactants both contribute to the negative temperature dependence of the rate coefficient, k_3. Again, a parameterized nonstatistical back flux model had to be formulated. Interestingly, the fitted back-flux parameter ($\gamma_0 \approx 1$) was the same as fitted for k_2. Finally, the clustering reaction of $FeO^+ + N_2O$ could be well-rationalized by standard unimolecular rate theory,[54,56] after the cluster dissociation energy was slightly increased over the value from DFT calculations. The modeling of this process confirmed that the reaction is close to the low pressure third-order limit under the experimental conditions of the present work. The modeling also allowed us to predict under which pressures a transition to the high pressure second-order range of the reaction is to be expected.

Acknowledgements

N.S.S. and A.A.V. are grateful for the support of the Air Force Office of Scientific Research for this work under Project AFOSR-2303EP. J.J.M. and S.G.A. acknowledge the support of the National Research Council. J.A.F. acknowledges the support of the Air Force Research Laboratory through the Space Scholars Program, as well as the Department of Defense for support through a National Defense Science and Engineering Graduate Fellowship. J.T. acknowledges support from the EOARD Grant Award FA8655-11-1-3077. J.L. and H.G. acknowledge support from the Department of Energy (DE-FG02-05ER15694).

References

1 K. Koszinowski, D. Schröder and H. Schwarz, *Organometallics*, 2004, **23**, 1132–1139.
2 G. A. Somorjai and J. Y. Park, *Phys. Today*, 2007, **60**, 48–53.
3 M. Schlangen and H. Schwarz, *Catal. Lett.*, 2012, **142**, 1265–1278.
4 D. K. Bohme and H. Schwarz, *Angew. Chem., Int. Ed.*, 2005, **44**, 2336–2354.
5 G. A. Somorjai and J. Y. Park, *Angew. Chem., Int. Ed.*, 2008, **47**, 9212–9228.
6 W. B. Tolman, *Angew. Chem., Int. Ed.*, 2010, **49**, 1018–1024.
7 M. M. Kappes and R. H. Staley, *J. Am. Chem. Soc.*, 1981, **103**, 1286–1287.
8 A. Burcat and B. Ruscic, Third Millenium Ideal Gas and Condensed Phase Thermochemical Database for Combustion with Updates from Active Thermochemical Tables, Technion-IIT, Aerospace and Engineering, Argonne National Laboratory, Chemistry Division, September 2005; ftp://ftp.technion.ac.il/pub/supported/aetdd/thermodynamics mirrored at http://garfiled.chem.elte.hu/Burcat/burcat.html (accessed August 2012), ANL-05/20 and TAE 960.
9 V. Baranov, G. Javahery, A. C. Hopkinson and D. K. Bohme, *J. Am. Chem. Soc.*, 1995, **117**, 12801–12809.
10 V. Blagojevic, G. Orlova and D. K. Bohme, *J. Am. Chem. Soc.*, 2005, **127**, 3545–3555.
11 V. V. Lavrov, V. Blagojevic, G. K. Koyanagi, G. Orlova and D. K. Bohme, *J. Phys. Chem. A*, 2004, **108**, 5610–5624.
12 P. B. Armentrout, L. F. Halle and J. L. Beauchamp, *J. Chem. Phys.*, 1982, **76**, 2449–2457.
13 G. Gioumousis and D. P. Stevenson, *J. Chem. Phys.*, 1958, **29**, 294–299.
14 J. M. C. Plane and R. J. Rollason, *J. Chem. Soc., Faraday Trans.*, 1996, **92**, 4371–4376.
15 Y. Shiota and K. Yoshizawa, *J. Chem. Phys.*, 2003, **118**, 5872–5879.
16 S. Chiodo, O. Kondakova, M. d. C. Michelini, N. Russo, E. Sicilia, A. Irigoras and J. M. Ugalde, *J. Phys. Chem. A*, 2004, **108**, 1069–1081.
17 D. Schröder, S. Shaik and H. Schwarz, *Acc. Chem. Res.*, 2000, **33**, 139–145.
18 J. M. Matxain, J. M. Mercero, A. Irigoras and J. M. Ugalde, *Mol. Phys.*, 2004, **102**, 2635–2637.
19 D. Schroder, H. Schwarz, D. E. Clemmer, Y.-M. Chen, P. B. Armentrout, V. Baranov and D. K. Bohme, *Int. J. Mass Spectrom. Ion Processes*, 1997, **161**, 175–191.
20 A. A. Viggiano, R. A. Morris, F. Dale, J. F. Paulson, K. Giles, D. Smith and T. Su, *J. Chem. Phys.*, 1990, **93**, 1149–1157.
21 P. B. Armentrout, *Annu. Rev. Phys. Chem.*, 1990, **41**, 313–344.
22 S. K. Loh, E. R. Fisher, L. Lian, R. H. Schultz and P. B. Armentrout, *J. Phys. Chem.*, 1989, **93**, 3159–3167.
23 E. R. Fisher, R. H. Schultz and P. B. Armentrout, *J. Phys. Chem.*, 1989, **93**, 7382–7387.
24 J. L. Elkind and P. B. Armentrout, *J. Phys. Chem.*, 1987, **91**, 2037–2045.
25 R. Liyanage and P. B. Armentrout, *Int. J. Mass Spectrom.*, 2005, **241**, 243–260.
26 P. A. M. van Koppen, M. T. Bowers, E. R. Fisher and P. B. Armentrout, *J. Am. Chem. Soc.*, 1994, **116**, 3780–3791.
27 R. H. Schultz and P. B. Armentrout, *J. Phys. Chem.*, 1987, **91**, 4433–4435.
28 J. J. Melko, S. G. Ard, J. A. Fournier, N. S. Shuman, J. Troe and A. A. Viggiano, *J. Phys. Chem. A*, 2012, **116**, 11500–11508.

29 P. A. M. Van Koppen, P. R. Kemper and M. T. Bowers, *J. Am. Chem. Soc.*, 1992, **114**, 10941–10950.
30 J. V. B. Oriedo and D. H. Russell, *J. Phys. Chem.*, 1992, **96**, 5314–5319.
31 J. L. Elkind and P. B. Armentrout, *J. Phys. Chem.*, 1986, **90**, 5736–5745.
32 S. D. Hanton, R. J. Noll and J. C. Weisshaar, *J. Phys. Chem.*, 1990, **94**, 5655–5658.
33 S. D. Hanton, R. J. Noll and J. C. Weisshaar, *J. Chem. Phys.*, 1992, **96**, 5176–5190.
34 T. Su and W. J. Chesnavich, *J. Chem. Phys.*, 1982, **76**, 5183–5185.
35 H. Jalink, F. Harren, D. van den Ende and S. Stolte, *Chem. Phys.*, 1986, **108**, 391–402.
36 F. Rondinelli, N. Russo and M. Toscano, *Inorg. Chem.*, 2007, **46**, 7489–7493.
37 K. R. S. Woodcock, T. Vondrak, S. R. Meech and J. M. C. Plane, *Phys. Chem. Chem. Phys.*, 2006, **8**, 1812–1821.
38 Y.-C. Wang, D.-P. Chen, Z.-Y. Geng and J.-H. Zhang, *J. Mol. Struct.*, 2008, **858**, 26–30.
39 C. Lee, W. Yang and R. G. Parr, *Phys. Rev. B: Condens. Matter Mater. Phys.*, 1988, **37**, 785–789.
40 A. D. Becke, *Phys. Rev. A: At., Mol., Opt. Phys.*, 1988, **38**, 3098–3100.
41 H.-J. Werner and P. J. Knowles, *J. Chem. Phys.*, 1985, **82**, 5053–5063.
42 H.-J. Werner, *Mol. Phys.*, 1996, **89**, 645–661.
43 J. D. Watts, J. Gauss and R. J. Bartlett, *J. Chem. Phys.*, 1993, **98**, 8718.
44 J. Sugar, *Atomic energy levels of the iron-period elements, potassium through nickel*, Published by the American Chemical Society and the American Institute of Physics for the National Bureau of Standards, New York, N.Y., 1985.
45 G. Nave and S. Johansson, *Astrophys. J., Suppl. Ser.*, 2013, **204**, 1.
46 M. J. Frisch, G. W. Trucks, H. B. Schlegel, G. E. Scuseria, M. A. Robb, J. R. Cheeseman, G. Scalmani, V. Barone, B. Mennucci, G. A. Petersson, H. Nakatsuji, M. Caricato, X. Li, H. P. Hratchian, A. F. Izmaylov, J. Bloino, G. Zheng, J. L. Sonnenberg, M. Hada, M. Ehara, K. Toyota, R. Fukuda, J. Hasegawa, M. Ishida, T. Nakajima, Y. Honda, O. Kitao, H. Nakai, T. Vreven, J. A. Montgomery, J. E. Peralta, F. Ogliaro, M. Bearpark, J. J. Heyd, E. Brothers, K. N. Kudin, V. N. Staroverov, R. Kobayashi, J. Normand, K. Raghavachari, A. Rendell, J. C. Burant, S. S. Iyengar, J. Tomasi, M. Cossi, N. Rega, J. M. Millam, M. Klene, J. E. Knox, J. B. Cross, V. Bakken, C. Adamo, J. Jaramillo, R. Gomperts, R. E. Stratmann, O. Yazyev, A. J. Austin, R. Cammi, C. Pomelli, J. W. Ochterski, R. L. Martin, K. Morokuma, V. G. Zakrzewski, G. A. Voth, P. Salvador, J. J. Dannenberg, S. Dapprich, A. D. Daniels, Ö. Farkas, J. B. Foresman, J. V. Ortiz, J. Cioslowski and D. J. Fox, *Gaussian 09, Revision B.01*, Wallingford, CT, 2009.
47 H. A. Olschewski, J. Troe and H. G. Wagner, *Ber. Bunsen-Ges. Phys. Chem.*, 1966, **70**, 450–459.
48 J. Troe and H. G. Wagner, *Ber. Bunsen-Ges. Phys. Chem.*, 1967, **71**, 937–979.
49 J. Troe, *J. Chem. Soc., Faraday Trans.*, 1994, **90**, 2303–2317.
50 J. Troe, *Int. J. Mass Spectrom. Ion Processes*, 1987, **80**, 17–30.
51 P. A. M. Van Koppen, J. Brodbelt-Lustig, M. T. Bowers, D. V. Dearden, J. L. Beauchamp, E. R. Fisher and P. B. Armentrout, *J. Am. Chem. Soc.*, 1990, **112**, 5663–5665.
52 J. Troe, *Chem. Phys. Lett.*, 1985, **122**, 425–430.
53 J. Troe, *J. Chem. Phys.*, 1996, **105**, 6249–6262.
54 T. Baer and W. L. Hase, *Unimolecular Reaction Dynamics: Theory and Experiments*, New York, Oxford, 1996.
55 M. Olzmann and J. Troe, *Ber. Bunsen-Ges. Phys. Chem.*, 1992, **96**, 1327–1332.
56 J. Troe and V. G. Ushakov, *J. Chem. Phys.*, 2011, **135**, 054304.
57 N. Eyet, N. S. Shuman, A. A. Viggiano, J. Troe, R. Relph, R. P. Steele and M. A. Johnson, *J. Phys. Chem. A*, 2011, **115**, 7582–7590.
58 R. D. Johnson III, ed., in NIST Standard Reference Database Number 101 Release 15b, http://cccbdb.nist.gov/.
59 Y. Luo, *Comprehensive Handbook of Chemical Bond Energies*, CRC Press, Boca Raton, FL, 2007.